RSC Applied Polymers

PAPER

View Article Online
View Journal

Cite this: DOI: 10.1039/d5lp00272a

A multifunctional thermochromic–elastomeric composite for integrated pressure and temperature sensing

Fatemeh Motaghedi, †[a] Lina Rose, †[a,b] Mohammed Jalal Ahamed, *[b] Tricia Breen Carmichael *[a] and Simon Rondeau-Gagné *[a]

The growing demand for flexible and multifunctional sensors has driven the development of functional materials that can simultaneously respond to multiple and diverse stimuli, including mechanical stress and changes in temperature. In this work, we report the development of a multifunctional composite dielectric material combining thermochromic polydiacetylene (PDA) and styrene–ethylene–butylene–styrene (SEBS) for use in flexible capacitive pressure sensors. To further enhance pressure sensitivity, the dielectric layer was patterned with Mesoamerican pyramid (MAP) microstructures, which amplify mechanical deformation and increase effective contact area. It also shows the soft molding fabrication capability of the composite. The composite demonstrates excellent mechanical resilience, maintaining stable capacitance over 10 000 loading cycles at 220 N, and exhibits thermally responsive behavior, with reversible color transitions at 45 °C and irreversible changes at 90 °C. The resulting sensors display reliable performance across a broad dynamic range of pressure and temperature, making them well-suited for applications in wearable electronics, biomedical monitoring, and smart human–machine interfaces. This work highlights the potential of combining structural patterning with functional composites to engineer responsive and robust soft sensing platforms.

Received 29th August 2025,
Accepted 10th December 2025

DOI: 10.1039/d5lp00272a

rsc.li/rscapplpolym

Introduction

Flexible sensors have emerged as indispensable components in modern healthcare and wearable technology due to their combined mechanical compliance, comfort, and sensing precision.[1–3] Engineered to detect a broad range of external stimuli and physiological signals, including temperature, pressure, strain, heart rate, and biochemical markers, these sensors are central to the evolution of next-generation flexible electronic systems.[4,5] Unlike traditional rigid and bulky sensing devices, flexible sensors are fabricated from soft, stretchable materials that can conform intimately to the contours of human skin or be seamlessly integrated into textiles.[6] This enables continuous, non-invasive, and real-time health monitoring with minimal discomfort or interference with daily activities.[7] Their adaptability not only improves user compliance and data accuracy but also opens new frontiers in personalized medicine, rehabilitation, and remote diagnostics.[8–10] As such, flexible sensors are transforming the landscape of digital health by enabling more responsive, intelligent, and user-friendly monitoring solutions.

Building on the growing integration of flexible sensors in health monitoring, recent technological advancements have made self-tracking of daily activities more accessible and seamless than ever before.[11–13] This practice relies on embedded sensors and analytical algorithms to collect, process, and visualize personal health data in real time.[14] Its adoption has surged, particularly in the domains of fitness, wellness, and preventative healthcare, as users seek greater control and insight into their physical well-being.[15] In the context of wearable health monitoring, physiological parameters such as pressure, temperature, and humidity are critical indicators that influence both bodily functions and daily well-being.[16,17] Traditionally, most wearable devices have relied on single-modal sensors, each designed to detect a specific stimulus, such as pressure, humidity, or temperature, with high sensitivity and reliability.[16] While effective in targeted applications, these sensors often provide a limited view of the complex interactions between multiple physiological and environmental factors.[18] In contrast, multi-modal sensors, which can simultaneously monitor several stimuli, offer a more holistic and accurate assessment of the user's condition

[a]Department of Chemistry and Biochemistry, University of Windsor, Ontario, Canada N9B 3P4. E-mail: srondeau@uwindsor.ca, tbcarmic@uwindsor.ca
[b]Department of Mechanical, Automotive and Materials Engineering, University of Windsor, Ontario, Canada N9B 3P4. E-mail: M.Ahamed@uwindsor.ca
† These authors contributed equally to this work as co-first authors.

and surroundings. By combining data streams from multiple parameters, multi-modal sensors enhance decision-making and enable more responsive and precise interventions.[19]

Many multifunctional sensors achieve their versatility by integrating multiple sensing modalities through the physical stacking of distinct sensing layers.[20,21] While this layered architecture allows simultaneous detection of various stimuli, it often increases device thickness, reduces flexibility, and complicates fabrication processes, factors that can be limiting for wearable and conformable applications. Moreover, stacked configurations are prone to signal crosstalk, where overlapping responses from different sensing units can interfere with accurate data interpretation.[16] To overcome these limitations, there is a growing emphasis on the development of advanced materials and architectures capable of intrinsically responding to multiple external stimuli, such as pressure, humidity, and temperature, within a single, unified sensing layer.[22–26] Such innovations are key to achieving compact, flexible, and crosstalk-free multi-modal sensors, paving the way for next-generation wearable systems with enhanced functionality, reliability, and user comfort. For instance, Yu *et al.* used Bi_2Te_3, known for its thermoelectric and piezoresistive properties, as the sensing material in a thermoelectric flexible temperature–pressure dual-modal sensor featuring a three-dimensional (3D) helical structure.[27] The sensor exhibited outstanding performance in both temperature sensitivity ($-426.4\ \mu V\ K^{-1}$) and pressure sensitivity ($120\ Pa^{-1}$). However, despite these significant advancements in structural design and material application, full decoupling of temperature and pressure signals remain a challenge. In another work, Meng *et al.* developed a dual-function flexible pressure and temperature sensor by printing a modified PEDOT:PSS layer onto a microstructured PDMS substrate.[28] The addition of dimethyl sulfoxide (DMSO) significantly enhanced the charge transport properties of PEDOT:PSS, making its resistivity unaffected by temperature fluctuations. As demonstrated in their study, the voltage between the electrodes responded exclusively to temperature changes, while the resistance signal was sensitive only to applied pressure, effectively achieving signal decoupling for simultaneous temperature and pressure detection.

Building on these advances in multifunctional materials and soft sensor platforms, we previously reported the synthesis of a 1,3-butadiyne-containing oligosiloxane and its solid-state photo crosslinking to form polydiacetylenes (PDAs), a well-known class of thermochromic polymers capable of responding to various external stimuli through characteristic colorimetric changes.[29] These hybrid materials showed an improved solubility in common organic solvents and enabled facile thin-film fabrication *via* solution processing. The resulting material exhibited reversible thermochromism, transitioning from blue to red in the 25–47 °C range. More importantly, we demonstrated the integration of these materials into dual-mode capacitive temperature sensors, achieving reliable optical and capacitive temperature readouts over a broad operational window (25–80 °C) in soft, flexible formats. While these results highlight the promise of organic hybrid materials for multifunctional sensing, the increasing demand for real-time, wearable diagnostics calls for the development of platforms that can simultaneously detect and decouple multiple stimuli within a single sensing unit. In particular, the integration of pressure and temperature sensing into one platform remains a key objective.[28]

Herein, we report the development of a dual-mode sensor capable of quantifying both temperature and pressure through integrated optical and electrical readouts. The sensor platform was fabricated by physically combining PDA-crosslinked oligosiloxanes with SEBS, yielding a soft, multifunctional material. To enable pressure sensing and enhance capacitive responsiveness under mechanical loading, we patterned the sensing layer with Mesoamerican pyramidal (MAP) structures, which can be readily replicated using low-cost, out-of-cleanroom fabrication methods.[30] Our results demonstrate that MAP-structured sensors exhibit markedly enhanced sensitivity and pronounced capacitance variation across a broad range of applied pressures. In particular, the sensors show excellent performance within the 0–480 N range, achieving a sensitivity of $68\ kPa^{-1}$. This high-pressure sensitivity, combined with stable and repeatable capacitance changes, highlights the potential of MAP structures for advanced sensing applications. Moreover, the sensors display a clear and reversible optical response, with a distinct color shift from blue to red as the temperature increases from room temperature to 45 °C. This thermochromic response allows for straightforward optical temperature sensing without the need for additional circuitry, offering a simple and accessible means of thermal monitoring. Our composite exhibits intrinsic multi-modal sensitivity derived from a single, structurally integrated material system. This design avoids the need for additional processing steps or alignment between layers, enabling simple fabrication and better mechanical integrity under deformation. Importantly, it also supports reliable decoupling of pressure and thermal stimuli, which is a persistent challenge in current multifunctional sensors.

Experimental section

Materials

SEBS H1052-901243 was purchased from Asahi Kasei. Purified P2-single-walled carbon nanotubes (SWCNTs) were sourced from Carbon Solutions (U.S.) and were treated with regioregular poly(3-hexylthiophene) (Ossila, U.S.) as a surfactant following reported procedures to produce conductive solution.[30] 1,3-Butadiyne-containing oligosiloxane was synthesized according to previous work.[30]

Measurements and characterizations

Fourier-transform Infrared (FT-IR) spectroscopy was performed using a Bruker Alpha spectrometer. Confocal Raman spectroscopy was carried out using a WiTec Raman system equipped with a 1064 nm laser source processed using Project

FOUR 4.0 software. UV-vis spectroscopy was performed on a Varian UV/Visible Cary 50 spectrophotometer.

SEBS–PDA composite and micropattern fabrication

To fabricate the device, SEBS (1 g) was dissolved in chloroform (5 mL) at 80 °C. Separately, the PDMS–PDA prepolymer (100 mg) was dissolved in chloroform (1 mL). The two solutions were then blended in a 5 : 1 ratio and stirred for approximately 30 minutes to ensure homogeneity. The resulting mixture was cast into a mold featuring Mesoamerican Pyramidal (MAP) patterns and placed in a desiccator to remove trapped air bubbles.[30] The mold was left to dry at room temperature, forming a flexible, microstructured film. Polymerization of the diacetylene units was initiated *via* UV irradiation at an intensity of 176 W m^{-2} (254 nm). Within 15 seconds of exposure, the film underwent a visible color change from transparent to blue, indicating successful formation of polydiacetylene.

Sensor fabrication

To prepare the conductive materials for the capacitor electrodes, P2SWCNT (7 mg) was dispersed in chloroform (30 mL) along with poly(3-hexylthiophene) (2 mg). The mixture was probe-sonicated for 30 minutes at 30% amplitude (75 W) to ensure uniform dispersion. Following sonication, the resulting solution was spray-coated onto SEBS films without microstructured patterns to generate the electrodes. Capacitor devices were then assembled by sandwiching a MAP-structured polymer composite film between two such electrodes, with the structured film serving as the dielectric layer (Fig. S1).

Results and discussion

The materials selected for this work, namely styrene–ethylene–butylene–styrene (SEBS) and polydiacetylene-crosslinked (PDA) oligosiloxanes, were deliberately chosen to synergistically combine mechanical flexibility with thermochromic and dielectric properties for dual-mode sensing *via* capacitance and colorimetric readouts. SEBS provides the elasticity, stretchability, and durability needed to form deformable yet robust sensor structures capable of withstanding repeated mechanical stress. The PDA network, generated through the topochemical photopolymerization of a 1,3-butadiyne-functionalized oligosiloxane precursor, imparts unique thermochromic behavior, enabling reliable and reversible color changes in response to temperature variations.[31] The integration of SEBS and PDA thus enables the creation of multifunctional sensors that offer both mechanical and optical sensing capabilities, while remaining compatible with low-cost, scalable, and solvent-based processing methods. As detailed in Experimental section and Supplementary Information, SEBS–PDA composites were prepared by solution blending, followed by casting into custom-made molds and UV irradiation at 254 nm in a curing oven. The resulting composites exhibited good mechanical integrity along with the characteristic blue color of the PDA phase (Fig. 1).

Upon preparation of the thermochromic dielectric composite, we investigated its integration into a capacitive pressure sensor. To enhance the performance of such sensors, patterned microstructures have been widely employed, as they can significantly increase sensitivity, improve compressibility, and amplify capacitance variation under applied load.[32–34] As extensively reported in the literature, structures ranging from ordered micropyramids to random textures, inspired by materials like sandpaper, can help enlarge the effective contact area and modulate mechanical deformation, both critical factors in achieving high responsiveness.[35] While random patterns offer simplicity of fabrication and tolerance to misalignment, ordered microstructures provide greater control over mechanical and electrical properties. Building on these principles, our group developed microstructured arrayed patterns featuring Mesoamerican pyramid (MAP) geometries.[30] This design combines the benefits of ordered structures with hier-

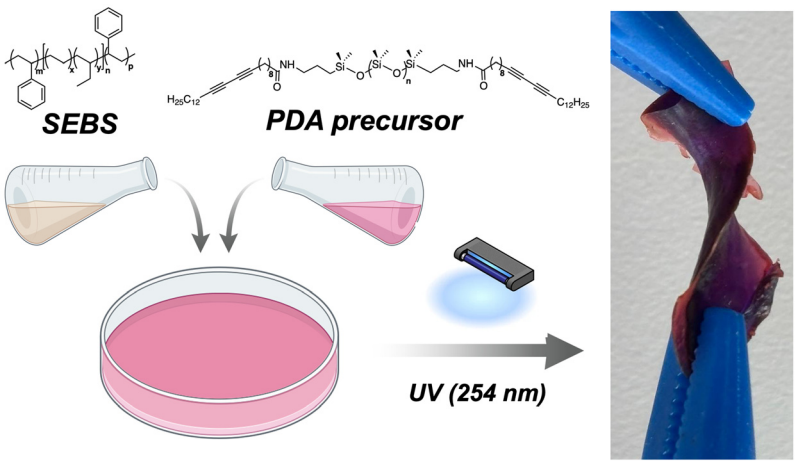

Fig. 1 Preparation of the thermochromic dielectric composite, combining SEBS with 1,3-butadiyne-containing oligosiloxane as polydiacetylene precursor.

archical features that promote enhanced deformation and capacitance changes across a wide pressure range. The MAP structures were fabricated using 3D-printed molds, allowing precise control over size and height, as detailed in Fig. 2a and Supplementary Information. The MAP structures remained intact upon irradiation with UV (254 nm) (Fig. 2b). Scanning electron microscopy (SEM) confirmed the uniformity and dimensions of the MAP-structured thermochromic dielectric layer, as shown in Fig. 2c and d. The MAPs exhibited a height of 1250 μm, a base width of 2100 μm, and an engineered inter-structural gap of 400 μm. To finalize the capacitor and further optimize the sensor performance, carbon nanotube (CNT) films were employed as flexible electrodes, leveraging their good electrical conductivity, thermal stability, and mechanical compliance. CNT films were deposited on SEBS substrates *via* spray coating, a versatile, low-cost, and scalable method compatible with various inks and substrates.[36]

In order to confirm the formation of PDA in the elastomeric matrix, the material was first characterized through Raman spectroscopy as this technique is widely used in literature for PDA-containing materials due to its particular sensitivity to alkyne and alkene functional groups.[37] Spectra of SEBS and the SEBS–PDA composite (before and after photoirradiation) were obtained using a laser excitation at 1064 nm. As illustrated in Fig. 3a (black curve), no peaks corresponding to alkyne or alkene are observed in the initial uncrosslinked composite. Upon photo-crosslinking, two new vibrations appear: a broad peak at 1453 cm^{-1} and another at 2081 cm^{-1} (blue curve). Both peaks are characteristic of the formation of PDA and can be attributed to the C=C and C≡C bonds in the PDA backbone, respectively. When the temperature is increased to 50 °C, both peaks exhibit a slight shift to 1512 cm^{-1} and 2118 cm^{-1}, accompanied by an observable color change from blue to red. These changes, typically observed for other types of PDA-based materials, can be attributed to the distortion of the ene-yne backbone from planarity in the polymer composite.[38] To further validate the Raman spectroscopy findings, Fourier-transform infrared (FTIR) spectroscopy was conducted, with results shown in Fig. S2. As FTIR is less sensitive to non-polar chemical bonds, the spectra of the SEBS–PDA composite in both the blue and red phases showed no significant differences. Even after heating the polydiacetylene above 50 °C to induce the blue-to-red transition, no additional spectral changes were observed. However, the SEBS–PDA composite exhibited a new peak around 1000 cm^{-1}, attributed to the oligosiloxane backbone, which confirmed the presence of the PDMS–PDA polymer. To further investigate the thermomechanical properties of the SEBS–PDA composite, thermogravimetric analysis (TGA) was first conducted. As shown in Fig. S3, both the pure SEBS and the composite exhibited similar thermal stability, with a 5% weight loss occurring around 400 °C, indicating the onset of thermal degradation.

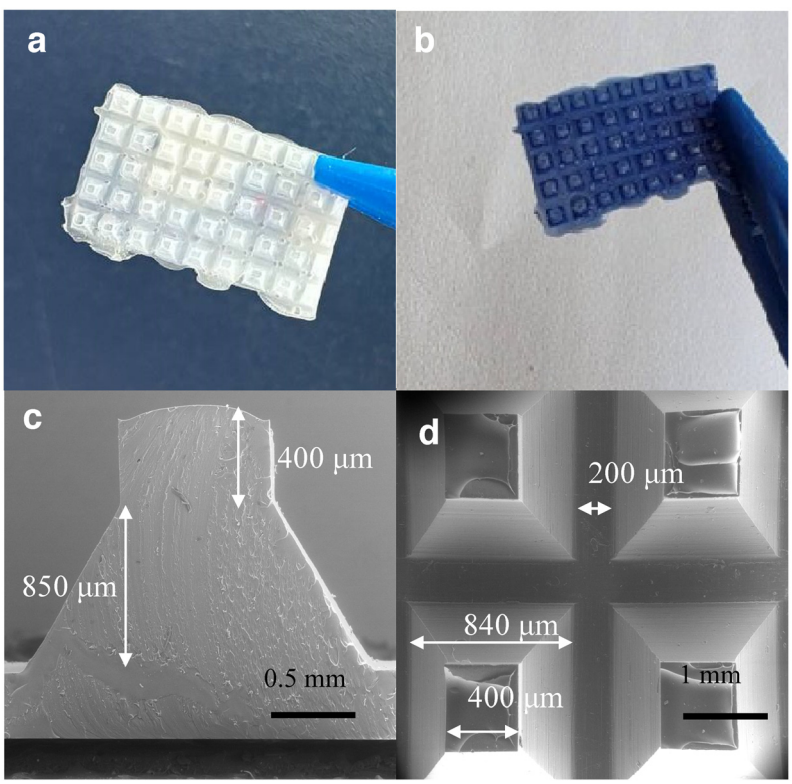

Fig. 2 Patterning of the SEBS–PDA composite. Photography of MAP-patterned dielectric materials (a) before and (b) after irradiation with UV (254 nm); scanning electron microscopy (SEM) image of (c) lateral and (d) cross-section of the MAP structure. Scale bars are respectively 0.5 and 1 mm.

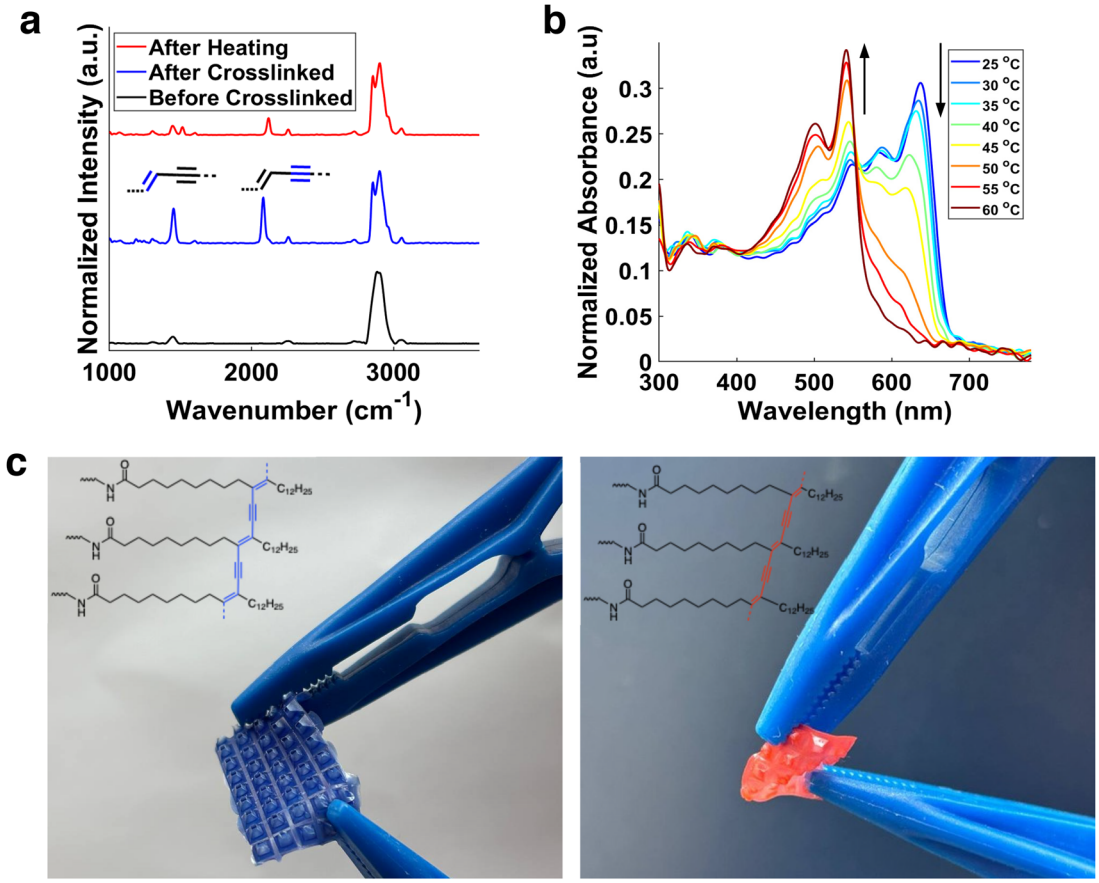

Fig. 3 Photocrosslinking of the composite. (a) Raman spectroscopy analysis for SEBS–PDA composite before crosslinked (black), after crosslinked (blue), polymer after heating (red); (b) UV-vis spectra of SEBS–PDA-crosslinked composite films from 25–60 °C, and (c) SEBS–PDA photocrosslinked composite before (left) and after (right) heating to 60 °C.

This suggests that the incorporation of the PDA-oligosiloxane network does not compromise the overall thermal stability of the elastomeric matrix. Differential scanning calorimetry (DSC) was subsequently performed to examine thermal transitions, with the corresponding thermograms presented in Fig. S4. Pristine SEBS displayed two characteristic features at −55.4 °C and 22.6 °C, corresponding to the glass transition and melting of the PEB mid-block, respectively. During cooling, crystallization of the PEB segments was observed at approximately 8.5 °C, in good agreement with previously reported values.[39] In the SEBS–PDA composite, similar SEBS-derived transitions were detected at −53.9 °C and 15.2 °C, reflecting the preserved thermal behavior of the host matrix. Notably, an additional endothermic event appears at ~47 °C. This transition, consistent with prior observations in related PDMS–PDA systems, can be attributed to irreversible chain twisting within the PDA domains and the associated thermochromic response of the composite film.

UV–vis spectroscopy was used to investigate the temperature-dependent optoelectronic properties of the SEBS–PDA composite, as shown in Fig. 3b. Upon heating the crosslinked SEBS–PDA thin films from room temperature to 60 °C, the absorption band associated with the blue phase at λ = 640 nm progressively decreased, while a new band emerged at λ = 540 nm, indicative of the formation of the red-phase PDA. Notably, this thermochromic transition was found to be irreversible above 45 °C; however, when heated to temperatures below this threshold, the color change remained fully reversible. These results align with previous reports highlighting the role of the oligosiloxane backbone in modulating the reversibility of thermochromism.[29] The corresponding visual color change is shown in Fig. 3c, and further discussion on thermochromism in polydiacetylenes can be found in previous literature.[40]

Building on the initial characterization and confirmation of its colorimetric temperature sensitivity, the SEBS–PDA composite was subsequently employed as a dielectric layer in a capacitive sensor. Designed to respond to both mechanical and thermal stimuli, this class of sensor has demonstrated utility in diverse applications, including soft electronics and environmental monitoring. To thoroughly assess the performance of the device and its constituent materials, systematic experiments were conducted under varying pressure and temperature conditions, focusing on pressure sensing behavior, thermal responsiveness, and durability under cyclic and environmental stress. The pressure sensitivity of the MAP-

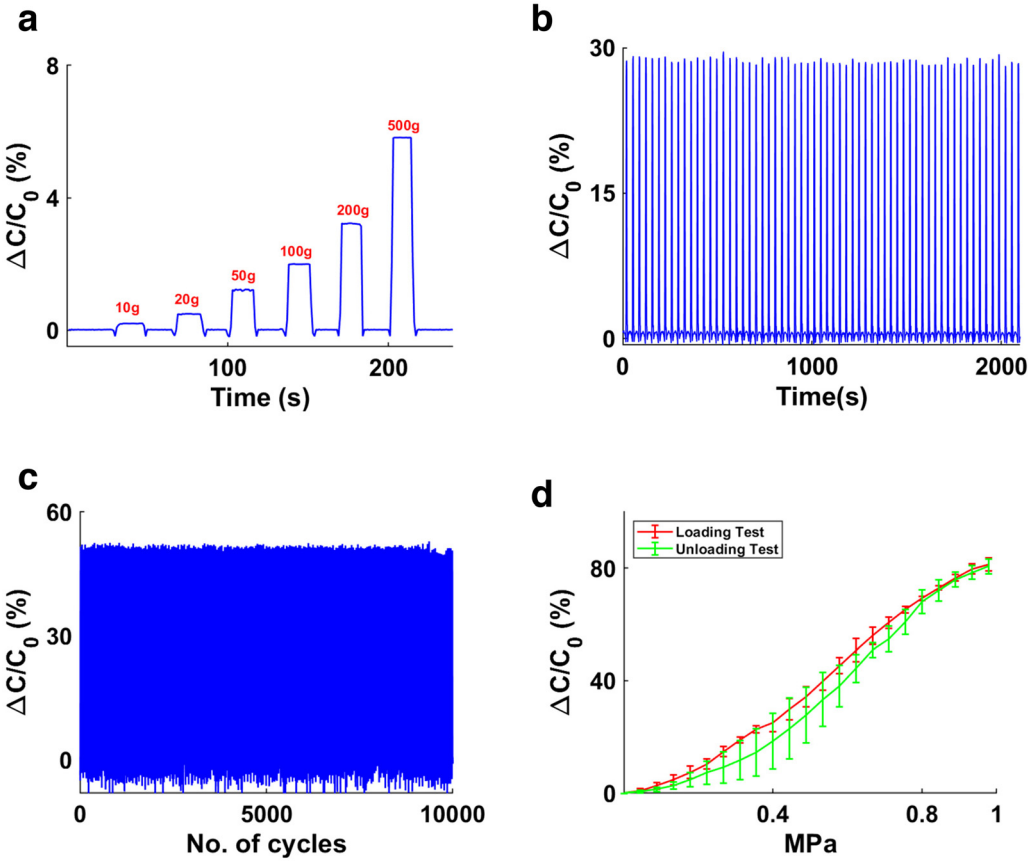

Fig. 4 Pressure sensing characteristics of the SEBS–PDA blend sensor at room temperature. (a) Relative capacitances change under ascending pressure (b) cyclic loading at 55 N; (c) fatigue tests at 220 N for 10 000 cycles, and (d) hysteresis plot for loading and unloading (0–480 N).

structured SEBS–PDA-based capacitor was first evaluated at constant temperature (room temperature), with experimental procedures detailed in the SI. As shown in Fig. 4a, the sensor exhibited a stepwise increase in relative capacitance change with increasing pressure using ascending weights ranging from 10 to 500 g (force less than 5 N). The signal remained stable at each pressure level, confirming the sensor's capability to distinguish discrete pressure inputs. To evaluate the sensor's mechanical resilience and repeatability, cyclic loading tests were conducted under a constant, moderate force of 55 N, as shown in Fig. 4b. This force was deliberately chosen to fall within the typical range of human interaction forces, such as firm finger presses or light gripping, which generally span from 30 N to 100 N.[41] This choice ensured that the testing conditions are representative of real-world scenarios relevant to wearable or biomedical applications. Under these conditions, the sensor demonstrated stable and repeatable performance over multiple cycles, confirming its robustness for practical use. To evaluate the sensor's behavior under high mechanical stress, a cyclic force of 220 N was applied, representative of forces commonly encountered in real-world scenarios such as leaning with one arm, sitting pressure, or localized contact during equipment handling. Under this load, the sensor underwent 10 000 repeated loading cycles, as shown in Fig. 4c. It maintained a consistent capacitance swing throughout the fatigue test, indicating minimal performance degradation and a stable electrode–dielectric interface. The sensor continued to exhibit a sharp and reproducible response, demonstrating reliable performance across a broad dynamic pressure range. The sensitivity increased slightly from 60.0 to 63.8 kPa^{-1}, which is about a 6.3% rise. This improvement is likely due to mechanical preconditioning, where repeated loading helps the microstructures settle into a better shape, improving contact and internal distribution of stress. In addition to durability and stability, the sensor also showed a response time of 0.54 seconds, further confirming its suitability for real-time pressure sensing. When looking at hysteresis (Fig. 4d), our results confirmed a nonlinear yet stable relationship between applied pressure (up to 450 N) and capacitance response. The curve showed a steep initial slope at low pressures, indicative of high sensitivity, followed by a gradual saturation at higher loads. Notably, standard deviation across repeated measurements remained stable, confirming reproducibility and a relatively low hysteresis.

The SEBS–PDA capacitive pressure sensors demonstrated reliable performance, comparable to other elastomer-based sensors using materials like PDMS.[34,42] Notably, the SEBS–

PDA composite with MAP structure withstood tensile strains over 60% without failure, while previously-reported MAP-patterned PDMS-based sensors fractured at 35–40%, indicating 1.5 to 1.7 times greater stretchability and superior mechanical flexibility.[30] However, the SEBS–PDA MAP sensor showed slightly lower pressure sensitivity (60 kPa^{-1}) than its PDMS counterpart (77 kPa^{-1}), confirming that sensitivity depends not only on elasticity but also on dielectric properties, internal air gaps, and baseline capacitance (Table S1). The SEBS–PDA MAP sensor also showed device characteristics comparable to other well-known soft pressure sensors (Table S2). Capacitance-time plots taken before and after the 10 000 cycles showed that the sensor response remained consistent, there was no loss in signal quality, no drift in baseline, and peak values stayed the same. This contrasts with the MAP–PDMS sensor, which showed a 12.8% drop in sensitivity under similar testing, indicating mechanical wear. Overall, these results show that the SEBS–PDA MAP sensor is not only more elastic and structurally stable, but it also improves slightly with repeated use. Its ability to maintain and even enhance sensitivity under both mechanical and thermal stress makes it highly suitable for long-term and high-temperature sensing applications.

To evaluate the thermal sensing capability and mechanical durability of the SEBS–PDA-based device, a series of temperature- and strain-dependent experiments were conducted, as depicted in Fig. 5. As shown in Fig. 5a, the sensor was initially loaded with a 500 g (5 N approximately) weight, and the temperature was subsequently increased from room temperature to 90 °C. This resulted in a smooth and consistent increase in capacitance, followed by a stable region, confirming the thermal stability of the dielectric layer. This response is likely due to the thermally activated softening of SEBS above 80 °C, where the solid film begins to deform and partially melt, resulting in a thinner dielectric layer. To compare the effects of pressure and temperature on the sensor with a dielectric composed of SEBS without PDA, similar test conditions were applied, as shown in Fig. 5b. In this case, the sensor was initially loaded with a 500 g weight, and the temperature was subsequently increased from room temperature to 90 °C. The results show that temperature has a significant effect on the capacitance compared to the SEBS–PDA composite. This behavior arises because SEBS deforms more easily under heat when it lacks the PDA precursor. Furthermore, the sensor exhibited poor reversibility; after the weight was removed, the capacitance did not return to its initial value. To further investigate the sensor's mechanical and thermal behavior, cyclic loading was performed at 220 N under two temperature conditions: 45 °C and 90 °C (Fig. 5c and d). To reflect practical usage scenarios, 45 °C was chosen to approximate elevated skin temperatures during extended contact in wearable and biomedical settings.[43,44] At 45 °C, the SEBS–PDA composite exhibited reversible thermochromic behavior, transitioning visibly from blue to red and returning upon cooling, demonstrating stable and repeatable thermal responsiveness (Fig. S5–9). Notably, although the CNT electrodes used in this study were not fully transparent, the chromic response remained visible through the surrounding SEBS matrix and from the edges of the dielectric layer where PDA was not obscured by the electrode footprint. Transparent electrode options such as ITO-coated PET can also be readily implemented, as demonstrated in our previous work, without altering the composite formulation.[29] In contrast, 90 °C was selected to probe sensor stability and functionality in high-temperature scenarios exceeding typical physiological exposure.[45] At this elevated temperature, the SEBS–PDA composite underwent an irreversible color change, indicating a permanent phase or molecular transition within the PDA domains. Moreover, SEBS starts to soften above 80 °C, and the MAP structure slowly disappears due to the heat (Fig. S10). As a result, the sensor deforms more with each cycle, which causes the capacitance to increase over time. Therefore, the effective operating temperature range of the device lies below the softening and melting transition of SEBS, approximately under 80 °C, where the material retains its mechanical integrity and the sensor delivers stable, reproducible performance without noticeable capacitance drift. This behavior delineates the upper thermal stability limit of the composite and provides critical insight into the sensor's reliable operational window for practical applications.[46,47] A combined pressure–temperature experiment (Fig. 5d) reveals a progressive increase in peak capacitance across cycles, suggesting a coupling effect in which the dielectric becomes more compressible at higher temperatures. Long-term durability was evaluated through cyclic tensile loading, with results shown in Fig. 5e. The sensor was repeatedly stretched from its initial length to 80% strain for 50 cycles without notable signal degradation. Instead, a gradual increase in response amplitude was observed, likely due to polymer relaxation or improved contact between the electrodes and dielectric over time. The mechanical robustness of the sensor was also confirmed under tensile conditions (Fig. 5f), with the same polymer sample exhibiting a Young's modulus of approximately 1.3 MPa. Notably, as shown in Fig. S11, the colorimetric response remained unchanged during mechanical stretching, confirming that the blue-to-red color transition is governed by temperature, not mechanical strain. To further validate this observation, UV-vis spectroscopy was performed on the composite under applied tensile strain. The resulting spectra (Fig. S12) showed no significant changes in absorption features associated with the PDA phase transition, confirming that strain alone does not affect the optical properties of the material. Taken together, these findings demonstrate that the SEBS–PDA composite sensor exhibits dual sensitivity to pressure and temperature, with strong repeatability, stability, and mechanical durability. Its nonlinear but predictable response across a wide range of conditions makes it well suited for both low- and high-pressure applications. The gradual, monotonic thermal response highlights its potential for integration into environmental or wearable sensing platforms.

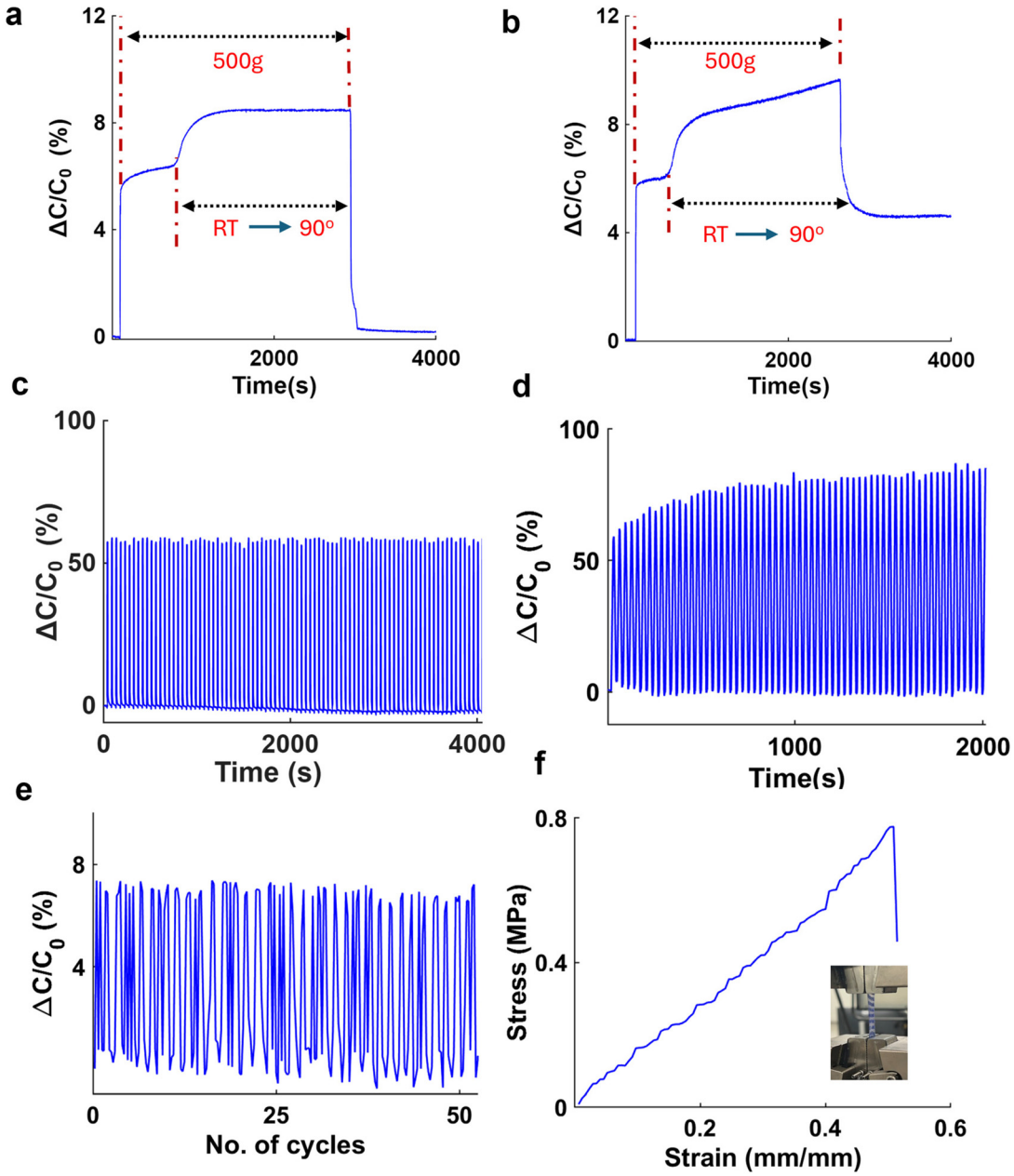

Fig. 5 Temperature Sensing Response and mechanical properties of the SEBS–PDA composite. (a) Relative change in capacitance during a gradual temperature increase from room temperature to 90 °C under a constant 500 g load; (b) Relative change in capacitance during a gradual temperature increase from room temperature to 90 °C under a constant 500 g for SEBS without PDA precursor (c) cyclic response at a constant 220N loading at 45 °C; (d) Cyclic response at constant 220N loading at 90 °C; (e) sensor stretched at 50 cycles using Velmex stretching stage, and (f) stress- strain curve analysis using INSTRON tensile measurement.

Conclusion

In summary, this work presents a multifunctional composite material that integrates mechanical resilience, thermal responsiveness, and pressure sensitivity into a single platform. By combining SEBS with thermochromic PDA, we developed a dielectric layer capable of withstanding extensive cyclic loading while exhibiting reversible color changes at physiologically relevant temperatures. To further enhance sensitivity in capacitive measurements, the composite material was patterned with Mesoamerican pyramid (MAP) structures, resulting in a structured dielectric layer optimized for pressure sensor applications. In addition to reversible thermochromism confirmed by UV-vis spectroscopy, the sensor demonstrated stable capacitive responses under both moderate and high mechanical stress, as well as under varying thermal conditions, confirming the robustness of the electrode–dielectric interface and the reliability of the composite system. Importantly, the

irreversible thermochromic behavior observed at elevated temperatures offers additional insight into the thermal limits of the material, which may inform future design considerations for application-specific deployment. Together, these results underscore the potential of SEBS–PDA composites for use in wearable electronics, smart biomedical devices, and soft robotics where integrated mechanical and thermal sensing is essential.

Author contributions

All authors contributed to the manuscript. All authors have approved to the final version of the manuscript.

Conflicts of interest

The authors declare no conflict of interest.

Data availability

The data supporting this article have been included as part of the supplementary information (SI). Supplementary information: detailed experimental procedures for all new compounds, and a complete characterization of materials and devices. See DOI: https://doi.org/10.1039/d5lp00272a.

Acknowledgements

This work was supported by NSERC through Discovery Grants (SRG: RGPIN-2022-04428, TBC: RGPIN-2018-05525, MJA: M.J.A: RGPIN-2023-03423). S. R-G. and T. B. C thank the Canadian Foundation for Innovation (CFI) for supporting the infrastructure used in this work.

References

1 Y. Huang, X. Fan, S.-C. Chen and N. Zhao, Emerging Technologies of Flexible Pressure Sensors: Materials, Modeling, Devices, and Manufacturing, *Adv. Funct. Mater.*, 2019, **29**, 1808509.
2 J.-H. Lee, K. Cho and J.-K. Kim, Age of Flexible Electronics: Emerging Trends in Soft Multifunctional Sensors, *Adv. Mater.*, 2024, **36**, 2310505.
3 M. Xie, K. Hisano, M. Zhu, T. Toyoshi, M. Pan, S. Okada, O. Tsutsumi, S. Kawamura and C. Bowen, Flexible Multifunctional Sensors for Wearable and Robotic Applications, *Adv. Mater. Technol.*, 2019, **4**, 1800626.
4 F. Xu, X. Li, Y. Shi, L. Li, W. Wang, L. He and R. Liu, Recent Developments for Flexible Pressure Sensors: A Review, *Micromachines*, 2018, **9**, 580.
5 T. Q. Trung and N.-E. Lee, Flexible and Stretchable Physical Sensor Integrated Platforms for Wearable Human-Activity Monitoringand Personal Healthcare, *Adv. Mater.*, 2016, **28**, 4338–4372.
6 Y. Zhang, H. Wang, H. Lu, S. Li and Y. Zhang, Electronic fibers and textiles: Recent progress and perspective, *iScience*, 2021, **24**, 102716.
7 V. T. N. Linh, S. Han, E. Koh, S. Kim, H. S. Jung and J. Koo, Advances in wearable electronics for monitoring human organs: Bridging external and internal health assessments, *Biomaterials*, 2025, **314**, 122865.
8 D. Chen and Q. Pei, Electronic Muscles and Skins: A Review of Soft Sensors and Actuators, *Chem. Rev.*, 2017, **117**, 11239–11268.
9 Q. Hua, J. Sun, H. Liu, R. Bao, R. Yu, J. Zhai, C. Pan and Z. L. Wang, Skin-inspired highly stretchable and conformable matrix networks for multifunctional sensing, *Nat. Commun.*, 2018, **9**, 244.
10 K. Xu, Y. Lu and K. Takei, Multifunctional Skin-Inspired Flexible Sensor Systems for Wearable Electronics, *Adv. Mater. Technol.*, 2019, **4**, 1800628.
11 S. Feng, M. Mäntymäki, A. Dhir and H. Salmela, How Self-tracking and the Quantified Self Promote Health and Well-being: Systematic Review, *J. Med. Internet Res.*, 2021, **23**, e25171.
12 D. Lupton and S. Maslen, The more-than-human sensorium: sensory engagements with digital self-tracking technologies, *Sens. Soc.*, 2018, **13**, 190–202.
13 M. Pantzar and M. Ruckenstein, Living the metrics: Self-tracking and situated objectivity, *Digital Health*, 2017, **3**, 2055207617712590.
14 W. Dong, L. Yang, R. Gravina and G. Fortino, ANFIS fusion algorithm for eye movement recognition via soft multifunctional electronic skin, *Inf. Fusion*, 2021, **71**, 99–108.
15 Y. Pang, Z. Yang, Y. Yang and T.-L. Ren, Wearable Electronics Based on 2D Materials for Human Physiological Information Detection, *Small*, 2020, **16**, 1901124.
16 J. Li, Z. Fang, D. Wei and Y. Liu, Flexible Pressure, Humidity, and Temperature Sensors for Human Health Monitoring, *Adv. Healthcare Mater.*, 2024, **13**, 2401532.
17 D. Dias and J. P. Silva Cunha, Wearable Health Devices—Vital Sign Monitoring, Systems and Technologies, *Sensors*, 2018, **18**, 2414.
18 R. Yang, W. Zhang, N. Tiwari, H. Yan, T. Li and H. Cheng, Multimodal Sensors with Decoupled Sensing Mechanisms, *Adv. Sci.*, 2022, **9**, 2202470.
19 I. You, D. G. Mackanic, N. Matsuhisa, J. Kang, J. Kwon, L. Beker, J. Mun, W. Suh, T. Y. Kim, J. B.-H. Tok, Z. Bao and U. Jeong, Artificial multimodal receptors based on ion relaxation dynamics, *Science*, 2020, **370**, 961–965.
20 G. B. Pradhan, S. Jeong, S. Sharma, S. Lim, K. Shrestha, Y. Lee and J. Y. Park, A Breathable and Strain-Insensitive Multi-Layered E-Skin Patch for Digital Healthcare Wearables, *Adv. Funct. Mater.*, 2024, **34**, 2407978.
21 C. Zhang, C. Liu, B. Li, C. Ma, X. Li, S. Niu, H. Song, J. Fan, T. Zhang, Z. Han and L. Ren, Flexible Multimodal Sensing System Based on a Vertical Stacking Strategy for Efficiently

Decoupling Multiple Signals, *Nano Lett.*, 2024, **24**, 3186–3195.

22 H. Dai, C. Zhang, C. Pan, H. Hu, K. Ji, H. Sun, C. Lyu, D. Tang, T. Li, J. Fu and P. Zhao, Split-Type Magnetic Soft Tactile Sensor with 3D Force Decoupling, *Adv. Mater.*, 2024, **36**, 2310145.

23 L. Chen, Y. Xu, Y. Liu, J. Wang, J. Chen, X. Chang and Y. Zhu, Flexible and Transparent Electronic Skin Sensor with Sensing Capabilities for Pressure, Temperature, and Humidity, *ACS Appl. Mater. Interfaces*, 2023, **15**, 24923–24932.

24 S. Xiao, Y. He, Y. Lu, X. Niu, Q. Li, J. Wu, D. Luo, F. Tian, G. Wan and H. Liu, An ultrasensitive flexible pressure, temperature, and humidity sensor based on structurally adjustable nano-through-hole array films, *J. Mater. Chem. C*, 2023, **11**, 12685–12697.

25 W. Yang, D. Pan, S. Liu, G. Jia, Y. Wang, H. Liu, C. Liu and C. Shen, Multifunctional Wearable Conductive Nanofiber Membrane with Antibacterial and Breathable Ability for Superior Sensing, Electromagnetic Interference Shielding, and Thermal Management, *Adv. Funct. Mater.*, 2025, **35**, 2414811.

26 G. Jia, X. Yue, L. Duan, R. Yin, C. Pan, H. Liu, C. Liu and C. Shen, Biomimetic Gradient Fibrous Aerogel Pressure Sensor Featuring Ultrawide Sensitive Range and Extraordinary Pressure Resolution for Machine Learning Enabled Posture Recognition, *Adv. Fiber Mater.*, 2025, **7**, 1632–1647.

27 H. Yu, Z. Hu, J. He, Y. Ran, Y. Zhao, Z. Yu and K. Tai, Flexible temperature-pressure dual sensor based on 3D spiral thermoelectric Bi2Te3 films, *Nat. Commun.*, 2024, **15**, 2521.

28 X. Meng, L. Mo, S. Han, J. Zhao, Y. Pan, F. Wang, Y. Fang and L. Li, Pressure-Temperature Dual-Parameter Flexible Sensors Based on Conformal Printing of Conducting Polymer PEDOT:PSS on Microstructured Substrate, *Adv. Mater. Interfaces*, 2023, **10**, 2201927.

29 F. Motaghedi, L. Rose, A. K. Sur, G. Garg, A. Nyayachavadi, M. J. Ahamed, T. B. Carmichael and S. Rondeau-Gagné, Polydiacetylene-Crosslinked Oligosiloxanes for Dual-Mode Temperature Sensing, *Adv. Mater. Technol.*, 2025, **10**, 2401354.

30 L. Rose, G. Nagesh, P. Das, D. Skaf, F. Motaghedi, S. Rondeau-Gagné and M. J. Ahamed, Exploring mesoamerican pyramidal micro-structures in soft capacitors for positive and negative pressure sensing, *Flexible Printed Electron.*, 2025, **10**, 025003.

31 A. D. Tjandra, A.-H. Pham and R. Chandrawati, Polydiacetylene-Based Sensors To Detect Volatile Organic Compounds, *Chem. Mater.*, 2022, **34**, 2853–2876.

32 S. Baek, H. Jang, S. Y. Kim, H. Jeong, S. Han, Y. Jang, D. H. Kim and H. S. Lee, Flexible piezocapacitive sensors based on wrinkled microstructures: toward low-cost fabrication of pressure sensors over large areas, *RSC Adv.*, 2017, **7**, 39420–39426.

33 J. Qin, L.-J. Yin, Y.-N. Hao, S.-L. Zhong, D.-L. Zhang, K. Bi, Y.-X. Zhang, Y. Zhao and Z.-M. Dang, Flexible and Stretchable Capacitive Sensors with Different Microstructures, *Adv. Mater.*, 2021, **33**, 2008267.

34 J. Pignanelli, K. Schlingman, T. B. Carmichael, S. Rondeau-Gagné and M. J. Ahamed, A comparative analysis of capacitive-based flexible PDMS pressure sensors, *Sens. Actuators, A*, 2019, **285**, 427–436.

35 Y. Gao, G. Yu, J. Tan and F. Xuan, Sandpaper-molded wearable pressure sensor for electronic skins, *Sens. Actuators, A*, 2018, **280**, 205–209.

36 M. C. Karlapudi, M. Vahdani, S. M. Bandari, S. Peng and S. Wu, A Comparative Study on the Effects of Spray Coating Methods and Substrates on Polyurethane/Carbon Nanofiber Sensors, *Sensors*, 2023, **23**, 3245.

37 D. J. Sandman and Y. J. Chen, Linear, non-linear and raman spectroscopy of polydiacetylenes, *Polymer*, 1989, **30**, 1027–1031.

38 D.-H. Park, J. Hong, I. S. Park, C. W. Lee and J.-M. Kim, A Colorimetric Hydrocarbon Sensor Employing a Swelling-Induced Mechanochromic Polydiacetylene, *Adv. Funct. Mater.*, 2014, **24**, 5186–5193.

39 F. Ciuprina, D. M. Panaitescu, L. Enache, C. M. Damian, R. M. Grigorescu, A. R. Gabor, C. A. Nicolae, C. L. Nistor and R. Trusca, Control of dielectric and mechanical properties of styrenic block copolymer by graphite incorporation, *Materials*, 2022, **15**, 7577.

40 T. Eaidkong, R. Mungkarndee, C. Phollookin, G. Tumcharern, M. Sukwattanasinitt and S. Wacharasindhu, Polydiacetylene paper-based colorimetric sensor array for vapor phase detection and identification of volatile organic compounds, *J. Mater. Chem.*, 2012, **22**, 5970–5977.

41 R. Figueroa-Jacinto, T. J. Armstrong and W. Zhou, Normal force distribution and posture of a hand pressing on a flat surface, *J. Biomech.*, 2018, **79**, 164–172.

42 J. Cui, B. Zhang, J. Duan, H. Guo and J. Tang, Flexible Pressure Sensor with Ag Wrinkled Electrodes Based on PDMS Substrate, *Sensors*, 2016, **16**, 2131.

43 D. R. Seshadri, R. T. Li, J. E. Voos, J. R. Rowbottom, C. M. Alfes, C. A. Zorman and C. K. Drummond, Wearable sensors for monitoring the physiological and biochemical profile of the athlete, *npj Digit. Med.*, 2019, **2**, 72.

44 M. N. Cramer, D. Gagnon, O. Laitano and C. G. Crandall, Human temperature regulation under heat stress in health, disease, and injury, *Physiol. Rev.*, 2022, **102**, 1907–1989.

45 A. Molina, K. P. Padmasree, V. Escobar-Barrios, A. I. Mtz-Enriquez, A. Zakhidov, A. Encinas and J. Oliva, A biodegradable and flexible temperature sensor supported on avocado peel and its enhancement of detection by sensitizing with the La0.5Sr0.5CoO3 perovskite, *Mater. Chem. Phys.*, 2022, **292**, 126786.

46 J. H. Laurer, R. Bukovnik and R. J. Spontak, Morphological Characteristics of SEBS Thermoplastic Elastomer Gels, *Macromolecules*, 1996, **29**, 5760–5762.

47 M. Taşdemir and E. Uluğ, Mechanical, Morphological and Thermal Properties of SEBS, SIS and SBR-type Thermoplastic Elastomers Toughened High Impact Polystyrene, *Polym.-Plast. Technol. Eng.*, 2012, **51**, 164–169.